ISSN 0169-6548
Report No. 93-7

Communications on Hydraulic and Geotechnical Engineering

A 3D Particle Model for Transport Problems in Transformed Coordinates

May 1993

D.W. Dunsbergen / G.S. Stelling

TU Delft
Delft University of Technology

Faculty of Civil Engineering

Delft University of Technology
Department of Civil Engineering
Hydraulic and Geotechnical Engineering Division
Hydromechanics Group

A 3D particle model

for transport problems

in transformed coordinates

D.W. Dunsbergen and G.S. Stelling

Report no. 93-7

Delft, may 1993

Abstract

In this report, transport problems are solved with a particle method that takes into account the Eulerian background flow field. Dispersion and other transport problems can be solved applying this model, as long as the corresponding transport process is formulated with a flux gradient relation, i.e., the advection-diffusion equation. The particle method has been made consistent with such a transport process. Since many 3D flow models are formulated in general coordinates, the 3D particle displacements are also given with respect to such a coordinate system. Analytical and numerical aspects of this particle method have been studied. The effectiveness of the method have been demonstrated with two academic test cases including streamlines in a recirculation zone and grid dependency in a discharge problem.

Contents

1 Introduction

Three-dimensional hydrodynamic simulations are often executed because of transport problems, such as water pollution due to sewer systems, many kind of outfall problems, oil spill problems, etcetera. These hydrodynamic simulations give insight in the water movement. Besides the water movement, a mathematical-physical description of the transport process is needed to develop a transport model that predicts the advection and dispersion of pollutants in water. Virtually all transport theories assume a linear gradient transport model, CORRSIN (1974). The corresponding equation is known as the advection-diffusion equation. It is widely accepted that the solution of this equation gives a sufficient insight in the advection and dispersion of the evolution of pollutant in water.

In many cases, the solution technique of the transport simulation is based upon Eulerian methods. Unfortunately, these methods have several drawbacks:

- To avoid negative concentrations, filter techniques have to be used which introduces numerical diffusion, e.g., Forester-filter, FORESTER (1977).
- In cases of high concentration gradients the Eulerian approach gives inaccurate results, DRONKERS *et al.* (1981).
- Using nonorthogonal transformation to represent the physical domain, e.g., the sigma-transformation, the correct formulation and discretization of the transport equation often provoke discussion, KESTER *et al.* (1989).

Another solution technique is known as the particle method. These methods are frequently used to simulate the dispersion of pollutants in water, HEEMINK (1990). These models consider particles that represent a certain amount of mass determined by the initial injected pollutant. The evolution of the concentration distribution is obtained by simulating sample paths of the particles, where each path represents an independent realization of the transport process. The sample paths determine a mass distribution, which approximates the concentration distribution of the pollutant. The drawbacks mentioned in the previous paragraph are easily overcome and the advantages of such a particle model are revealed at discharge problems and other applications where high concentration gradients are present, such as local simulation of dispersion of pollutants in a course grid. Negative concentrations can not occur and the simplicity of the method makes it easy to implement the method on a digital computer.

This report will focus on such a particle method, while taking into account the following aspects:

(i) consistency with the advection-diffusion equation,
(ii) the flow field obtained with a 3D hydrodynamic free surface flow model in transformed coordinates, and
(iii) the numerical implementation of:
    1) the initial condition,
    2) an accurate advection step, and
    3) the dispersive step.

In section 2, two question will be discussed:

1) How to formulate a particle method such that consistency with a solution technique for the advection-diffusion equation is guaranteed?
2) How to compute the particle trajectories using the Eulerian flow information?

These two questions are solved with respect to a Cartesian coordinate system (section 2.1), a curvilinear coordinate system (section 2.2) and a free-surface flow application including the sigma-transformation (section 2.3).

The numerical implementation of the method is described in section 3. The numerical aspects will be illustrated with some experiments in section 4.

2. *The Particle Method; Consistency*

The advection-diffusion equation describes the transport of mass due to advection and as a result of random molecular motions (diffusion). In transport models the averaged turbulent transport is modelled similar to molecular diffusion, and also ends up with an advection-diffusion equation. Referring to Fick's law and the conservation of mass, this equation in an anisotropic medium reads, FISCHER *et al.* (1979):

$$\frac{\partial C}{\partial t} = -\sum_{i=1}^{3} \frac{\partial}{\partial x_i}(u_i C) + \sum_{i=1}^{3}\sum_{j=1}^{3} \frac{\partial}{\partial x_i}(D_{ij}\frac{\partial C}{\partial x_j}) \tag{2.1}$$

with C the concentration of transported substance, u_i the local flow velocity in x_i-direction and D_{ij} the diffusion coefficient, the rate of dispersal of the contaminant in x_i-direction due to the component of concentration gradient in x_j-direction.

The given approach of the advection-diffusion problem has been made from an 'Eulerian' point of view. It is also possible to make use of a 'Lagrangian' viewpoint. Then the history of particle movements will be investigated instead of the concentration and flux at fixed points in space. The consistency of such a statistical approach with the Eulerian approach expressed in (2.1) will be discussed in section 2.1, 2.2 and 2.3, including various coordinate systems. The Lagrangian method requires the statistical theory of Brownian motion. An introduction to these stochastic processes can be found in e.g., KARLIN and TAYLOR (1975), ARNOLD (1974) or JAZWINSKI (1970).

2.1 *The Particle Method in Cartesian Coordinates*

When macroscopic particles are moving in a fluid, the molecules of the surrounding fluid will collide with the particles causing random displacements of the particles. The migration and fluctuation in the displacement of the particles can be represented with a so-called Langevin equation, written as, i=1,2,3, RISKEN (1984):

$$\frac{d}{dt}(X_i) = h_i(\underline{X},t) + \sum_{j=1}^{3} g_{ij}(\underline{X},t)\Gamma_j(t) \tag{2.2}$$

with $\underline{X} = (X_1,X_2,X_3)^T$ the position of a particle, $\underline{h}$ the drift vector and g the noise tensor. The superscript T indicates the transpose of the vector. The stochastic Langevin force Γ_j is assumed to have zero mean and a Gaussian distribution with δ-correlation (Gaussian white noise, KAMPEN (1981b)). White noise does not exist in the real world, because it has a constant spectral density on the entire real axis, which implies that the associate energy becomes infinite. It is however a useful mathematical idealization for describing random influences. The process expressed in (2.2) can also be presented as a fluctuation equation, written as, i=1,2,3:

$$dX_i = h_i(\underline{X},t)dt + \sum_{j=1}^{3} g_{ij}(\underline{X},t)\, dW_j(t) \tag{2.3}$$

where equation (2.3) introduces the Wiener process $W_j(t)$, also referred to as the Brownian motion process, JAZWINSKI (1970).

Particle displacements can now be computed by integration of the stochastic differential equation (2.2). Time integration of equation (2.2) over the interval (t_0,t), means that (t_0,t) is divided into N intervals (t_n,t_{n+1}) of length Δt with $t_n = t_0 + n\Delta t$, $t_N = t$, $N\Delta t = t - t_0$ and the solution is obtained by successive summation over n of the integrand multiplied by Δt evaluated at $t_n + \alpha\Delta t$, $0 \le \alpha \le 1$. The integrand is Riemann integrable, if the sum converges to a certain limit, irrespective of α, i.e., irrespective of the evaluating point inside the interval. Here (2.2) represents a stochastic differential equation and $\Gamma_j(t)$ is neither mean square Riemann integrable, nor Riemann integrable with probability 1, see KARLIN and TAYLOR (1975). The solution depends on the choice of α and equation (2.2) becomes meaningful if the integration method is prescribed. The choice of this prescription gives rise to the Itô-Stratonovich problem, KAMPEN (1981b). The difference between the Itô and the Stratonovich procedure can be understood by looking again at equation (2.2). Since the strength of the fluctuation in the position of the particle $(\sum_{j=1}^{3} g_{ij}(\underline{X},t)\Gamma_j(t))$ depends on the position of the particle $(\underline{X})$, one has to decide whether the jump depends on the position before the jump ($\alpha = 0$ implies Itô) or after the jump ($\alpha = 0.5$ implies Stratonovich), see DURBIN (1983). When the equations are nonlinear the results of the Itô calculus differ from the results of the Riemann calculus.

Now the integration rule determines the properties of the stochastic process (2.2). Since the Itô interpretation yields an explicit method, the Itô calculus has been chosen to compute the particle displacements. Then the fluctuation equation (2.3) gives rise to a stochastic description of a probability density function which defines the probability to find a particle in an infinitesimal interval at time t per unit volume. The conditional probability density function of the particle positions, given the measurements, i.e., initial condition, embodies all the information of the state of the system (Bayesian or probabilistic viewpoint). The final description is governed by the so-called Fokker-Planck equation, RISKEN (1984) or KAMPEN (1981a). The three-dimensional Fokker-Planck equation is given in FELLER (1971), and reads:

$$\frac{\partial p}{\partial t} = -\sum_{i=1}^{3} \frac{\partial}{\partial x_i}(A_i p) + \sum_{i=1}^{3}\sum_{j=1}^{3} \frac{\partial^2}{\partial x_i \partial x_j}(B_{ij} p) \tag{2.4}$$

with $p = p(\underline{X},t\,|\,\underline{X}(t_0),t_0)$ the transition probability density function with $\underline{X}(t_0)$ the initial condition at time $t = t_0$, $\underline{A}$ the drift vector and $\underline{B}$ the noise tensor. Note that in fact, the equation should be referred to as the Itô-Fokker-Planck equation, to emphasize that the Itô integration rule has been used. It might seem that the choice of using the Itô or Stratonovich calculus is not based upon physical arguments. It is however stated that both integration rules are correct. It only leads to different Fokker-Planck equations. To guarantee consistency, the Fokker-Planck equation must be matched with the advection-

diffusion equation, which is based upon physical arguments. A different integration rule ends up with a different drift, h_i, and stochastic influence, g_{ij}, expressed in the local flow velocity, u_i, and diffusion coefficients, D_{ij}.

Prescribing the Itô integration rule, the matching procedure is continued. The coefficients showing up in (2.3) and (2.4) are related as follows, UFFINK (1990):

$$\begin{cases} h_i = A_i \\ \frac{1}{2}\sum_{k=1}^{3} g_{ik}g_{jk} = B_{ij} \end{cases} \tag{2.5a}$$

The analogy of equation (2.4) with the advection-diffusion equation (2.1) is obvious. Now the coefficients of the fluctuation equation (2.3) can be properly expressed in terms of the local flow velocity and the diffusion coefficients, such that consistency is guaranteed. So, in order to simulate a particle trajectory, determined by (2.3), h_i and g_{ij} must satisfy the following equations:

$$\begin{cases} h_i = u_i + \sum_{j=1}^{3} \frac{\partial D_{ij}}{\partial x_j} \\ \frac{1}{2}\sum_{k=1}^{3} g_{ik}g_{jk} = D_{ij} \\ p = C \end{cases} \tag{2.5b}$$

Finally the particle method is defined as a summation of successive particle displacements. Each displacement consists of a deterministic part and a stochastic part. The simulation is performed at discrete times, say $t_0 + n\Delta t$, with Δt the chosen time step. Without loss of generality, t_0 is set to zero and the transition from state $n\Delta t$ to state $(n+1)\Delta t$ is written as, i=1,2,3:

$$\Delta X_i^{(n)} = X_i^{(n+1)} - X_i^{(n)} = h_i(\underline{X}^{(n)}, n\Delta t)\Delta t + \sum_{j=1}^{3} g_{ij}(\underline{X}^{(n)}, n\Delta t)\Delta W_j(n\Delta t) \tag{2.6a}$$

The superscript between parentheses denotes the number of evolved time steps; $\underline{X}^{(n)}$ denotes $\underline{X}(n\Delta t)$. ΔW_j is simulated by a Gaussian number generator, with

$$\begin{aligned} E[\Delta W_j] &= 0 \\ E[\Delta \underline{W} \Delta \underline{W}^T] &= I\Delta t \end{aligned} \tag{2.6b}$$

and I the identity mapping.

Because the displacement of the particle contains a stochastic contribution, the particle method is also often referred to as the random walk method.

2.2. The Particle Method in Curvilinear Coordinates

The description of the random walk method in general coordinates can be obtained in two different ways. The discrete fluctuation equation can be transformed or the transformed Fokker-Planck equation can be matched with the transformed advection-diffusion equation. Both derivations have to yield the same result. Both ideas will be studied. It results in a description of the random walk method which can be implemented directly on a digital computer. The mutual connections between the equations are summarized in the figure depicted below. The figure expresses that the advection-diffusion equation and the Fokker-Planck equation have to be consistent. To derive a transformed random walk formulation, two routes are sketched:

(1) Fokker-Planck equation in Cartesian coordinates → Random walk in Cartesian coordinates → Transformed random walk
(2) Fokker-Planck equation in Cartesian coordinates → Transformed Fokker-Planck equation → Transformed random walk.

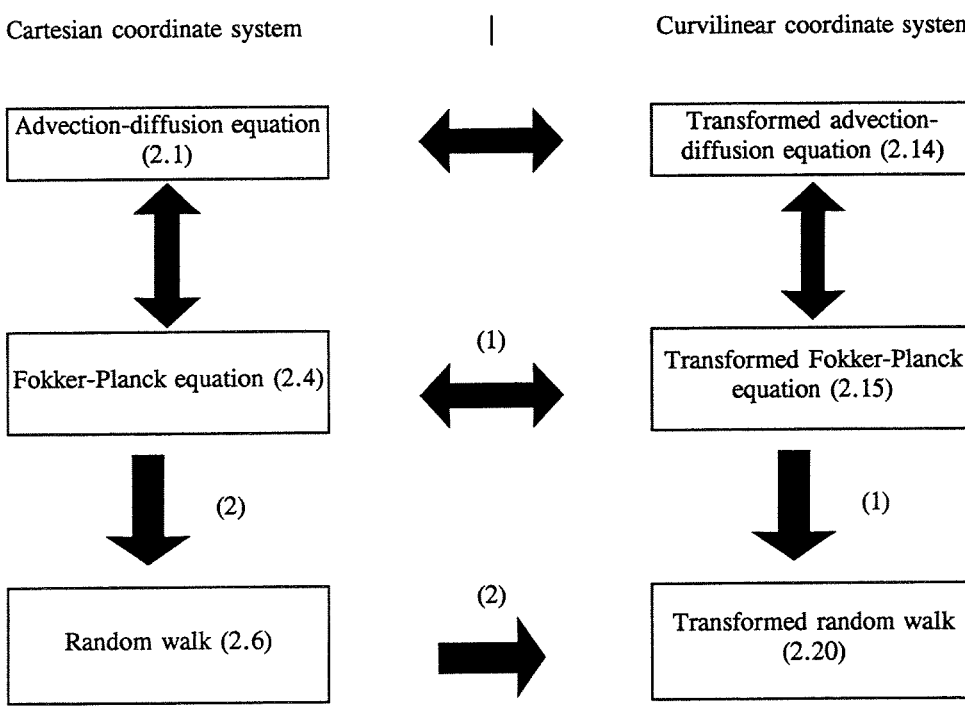

The objective is to derive the explicit expressions for the particle displacements in terms of the local flow velocity and the diffusion coefficients relative to a nonorthogonal curvilinear moving grid.

Since transformation relations are of interest, some relevant remarks about

transformation relations and the used notation, will be summarized in section 2.2.1. The necessary computational results are moved to appendix A.

2.2.1 Transformation Relations

Consider a transformation from a Cartesian coordinates system (x_1,x_2,x_3) to a general curvilinear system (ξ^1,ξ^2,ξ^3). The covariant base vectors, $\underline{a}_i$, the tangent vectors to the three coordinate lines, and the contravariant base vectors, $\underline{a}^i$, the normal vectors on the three coordinates surfaces ξ^i = constant , are written as (i=1,2,3):

$$\begin{aligned} \underline{a}_i^T &= \left(\frac{\partial x_i}{\partial \xi^1} , \frac{\partial x_i}{\partial \xi^2} , \frac{\partial x_i}{\partial \xi^3} \right) \\ \underline{a}^i &= \frac{1}{\sqrt{G}} \left(\underline{a}_j \wedge \underline{a}_k \right) \qquad \text{(i,j,k) cyclic} \\ \sqrt{G} &= | \underline{a}_1 \cdot (\underline{a}_2 \wedge \underline{a}_3) | \end{aligned} \tag{2.7}$$

with $\wedge$ the vector product sign. $\sqrt{G}$ represents the jacobian of the transformation, defined as a triple scalar product. The dot stands for the scalar product and $|\cdot|$ denotes the Euclidean norm.

Both coordinates $(\underline{x})$ and velocity $(\underline{u})$ are being transformed. Many flow models make use of grid-oriented, so-called contravariant velocity components (U^i) defined as, i=1,2,3:

$$U^i = \underline{a}^i \cdot \left(\underline{u} - \left(\frac{\partial \underline{x}}{\partial t} \right)_{\underline{\xi}} \right) \tag{2.8}$$

which represents the velocity component in ξ^i-direction relative to the moving grid. The subscript indicates the variable which is held constant. For a treatment of coordinate transformations, see THOMPSON *et al.* (1985) or CUVELIER (1987).

2.2.2 Particle Displacement in the Transformed Space

A particle displacement in the original space is denoted with $d\underline{X} = (dX_1,dX_2,dX_3)^T$, and the displacement in the transformed space with $d\underline{\Xi} = (d\Xi^1,d\Xi^2,d\Xi^3)^T$. The tensor analysis provides that the following deterministic equations are equivalent:

$$\frac{d\underline{X}}{dt} = \underline{u} \quad \Leftrightarrow \quad \frac{d\underline{\Xi}}{dt} = \underline{U} \tag{2.9}$$

Such a deterministic expression can not be used to compute the total displacement of a random walker in the transformed space. For the stochastic differential equation (2.2), the stochastic chain rule must be applied, see KLOEDEN and PLATEN (1992). In correspondence with equation (2.3), i=1,2,3:

$$d\Xi^i = \tilde{h}_i(\underline{X},t)dt + \sum_{j=1}^{3} \tilde{g}_{ij}(\underline{X},t)dW_j(t) \tag{2.10}$$

The transformed drift, $\tilde{h}_i$, and the transformed stochastic forcing, $\tilde{g}_{ij}$, are derived by inserting a Taylor series expansion in:

$$\Delta\underline{\xi} = \underline{\xi}(\underline{x} + \Delta\underline{x}, t + \Delta t) - \underline{\xi}(\underline{x},t) \tag{2.11}$$

Doing so, the transformed drift components become, for i=1,2,3:

$$\begin{aligned}\tilde{h}_i = {} & \underline{a}^i \cdot \left(\underline{u} - \left(\frac{\partial \underline{x}}{\partial t}\right)_{\underline{\xi}} \right) + \sum_{j=1}^{3}\sum_{k=1}^{3}\sum_{l=1}^{3} (\underline{a}^i)_l (\underline{a}^j)_k \frac{\partial D_{lk}}{\partial \xi^j} \\ & + \sum_{j=1}^{3}\sum_{k=1}^{3}\left(\sum_{l=1}^{3} (\underline{a}^l)_j \frac{\partial}{\partial \xi^l}\left[(\underline{a}^i)_k\right] \right) D_{jk}\end{aligned} \tag{2.12}$$

The latter contribution, i.e., the curvature term, results from the stochastic chain rule. This stochastic chain rule takes into account that $E[dWdW] = dt$. As a consequence, this first order term may not be neglected. The transformed noise components satisfy, for i=1,2,3, j=1,2,3:

$$\tfrac{1}{2}\sum_{k=1}^{3} \tilde{g}_{ik}\tilde{g}_{jk} = \sum_{k=1}^{3}\sum_{l=1}^{3} (\underline{a}^i)_k (\underline{a}^j)_l D_{kl} \tag{2.13}$$

Here it is concluded that as soon as the velocity components, the contravariant base vectors, the diffusion coefficients and the moving grid relations are known, the particle trajectory can be computed with respect to the computational domain. If the hydrodynamic model, that gave rise to the transformation, computes the contravariant velocity components, these components can easily be used to compute the deterministic displacement, as expressed in (2.12).

2.2.3 Relation with the Transformed Fokker-Planck Equation

In section 2.1, particle displacements have been derived by matching the advection-diffusion equation with the Fokker-Planck equation with respect to the Cartesian coordinate system. In the transformed space an analogue procedure can be followed. Appendix A gives the derivation of the transformed advection-diffusion equation and the transformed Fokker-Planck equation. The results from appendix A are copied here. The

transformed advection-diffusion equation reads:

$$\frac{\partial C}{\partial t} - \frac{1}{\sqrt{G}}\left(\frac{\partial \underline{x}}{\partial t}\right)_{\underline{\xi}} \cdot \sum_{i=1}^{3} \frac{\partial}{\partial \xi^i}[\sqrt{G}\underline{a}^i C] + \frac{1}{\sqrt{G}} \sum_{i=1}^{3} \frac{\partial}{\partial \xi^i}[\sqrt{G}\underline{a}^i \cdot \underline{u} C] = \sum_{i=1}^{3}\sum_{j=1}^{3}\sum_{k=1}^{3}\sum_{l=1}^{3} (\underline{a}^l)_i \frac{\partial}{\partial \xi^i}[(\underline{a}^k)_j D_{ij} \frac{\partial C}{\partial \xi^k}] \tag{2.14}$$

and the transformed Fokker-Planck equation,

$$\frac{1}{\sqrt{G}}\left(\frac{\partial(\sqrt{G}p)}{\partial t}\right)_{\underline{\xi}} = -\frac{1}{\sqrt{G}} \sum_{i=1}^{3} \frac{\partial}{\partial \xi^i}\left[\left(\sum_{j=1}^{3} (\underline{a}^i)_j A_j + \left(\frac{\partial \xi^i}{\partial t}\right)_{\underline{x}}\right)\sqrt{G}p\right] + \frac{1}{\sqrt{G}} \sum_{i=1}^{3}\sum_{j=1}^{3}\left(\sum_{k=1}^{3}\sum_{l=1}^{3} \frac{\partial}{\partial \xi^k}\left[(\underline{a}^k)_j \frac{\partial}{\partial \xi^l}\left((\underline{a}^l)_i B_{ij}\sqrt{G}p\right)\right]\right) \tag{2.15}$$

These two equations are again matched by putting, as in equation (2.5), for i=1,2,3 and j=1,2,3:

$$\begin{cases} \sqrt{G}p = C \\ A_i = u_i + \sum_{j=1}^{3} \frac{\partial D_{ij}}{\partial x_j} \\ B_{ij} = D_{ij} \end{cases} \tag{2.16}$$

To show that (2.15) defines the Fokker-Planck equation that corresponds with the process given in (2.10), equation (2.15) is written as:

$$\frac{\partial \tilde{p}}{\partial t} = -\sum_{i=1}^{3} \frac{\partial}{\partial \xi^i}(\tilde{A}_i \tilde{p}) + \sum_{i=1}^{3}\sum_{j=1}^{3} \frac{\partial^2}{\partial \xi^i \partial \xi^j}(\tilde{B}_{ij}\tilde{p}) \tag{2.17}$$

Equation (2.17) matches (2.15) if

$$\begin{cases} \tilde{p} = \sqrt{G}p \\ \tilde{A}_i = \left(\frac{\partial \xi^i}{\partial t}\right)_{\underline{x}} + \sum_{j=1}^{3} (\underline{a}^i)_j A_j + \sum_{j=1}^{3}\sum_{k=1}^{3} \frac{\partial^2 \xi^i}{\partial x_j \partial x_k} B_{jk} \\ \tilde{B}_{ij} = \sum_{k=1}^{3}\sum_{l=1}^{3} (\underline{a}^i)_k (\underline{a}^j)_l B_{kl} \end{cases} \tag{2.18}$$

Now, it is readily shown that

$$\begin{cases} \tilde{A}_i = \tilde{h}_i \\ \tilde{B}_{ij} = \tfrac{1}{2}\sum_{k=1}^{3} \tilde{g}_{ik}\tilde{g}_{jk} \end{cases} \tag{2.19}$$

This proves the statement that the Fokker-Planck equation that corresponds with equation (2.10) is given by (2.15).

2.2.4 *Summary of the Particle Displacements of a Particle Method in a Transformed Space*

As proved in the previous sections, a random walk in a transformed space can be formulated in terms of particle displacements. In order to guarantee consistency with the advection-diffusion equation (2.1), a particle displacement, $\Delta \underline{\Xi}$, per time step Δt satisfies, for i=1,2,3:

$$\begin{aligned} \Delta \Xi^i = \underline{a}^i \cdot \left(\underline{u} - \left(\frac{\partial \underline{x}}{\partial t} \right)_{\underline{\xi}} \right) \Delta t + \sum_{j=1}^{3}\sum_{k=1}^{3}\sum_{l=1}^{3} (\underline{a}^i)_l (\underline{a}^j)_k \frac{\partial D_{lk}}{\partial \xi^j} \Delta t \\ + \sum_{j=1}^{3}\sum_{k=1}^{3}\left(\sum_{l=1}^{3} (\underline{a}^l)_j \frac{\partial}{\partial \xi^l}\left[(\underline{a}^i)_k \right] \right) D_{jk} \Delta t \\ + \sum_{j=1}^{3} \tilde{g}_{ij} \Delta W_j \end{aligned} \tag{2.20a}$$

and $\tilde{g}_{ij}$ satisfying, for i=1,2,3, j=1,2,3:

$$\tfrac{1}{2}\sum_{k=1}^{3} \tilde{g}_{ik}\tilde{g}_{jk} = \sum_{k=1}^{3}\sum_{l=1}^{3} (\underline{a}^i)_k (\underline{a}^j)_l D_{kl} \tag{2.20b}$$

The quantities at the right-hand side of (2.20a) are evaluated at time $n\Delta t$, similar to an Euler explicit integration procedure, which corresponds with the Itô integration rule.

It is noted that with $\underline{a}^i = \underline{e}^i$, the unit Cartesian base vectors, equation (2.20a) reduces to (2.6a).

The hydrodynamic model produces the necessary estimates for the input quantities, such as the local flow velocity, $\underline{u}$ (or the contravariant velocity $\underline{U}$, given by (2.8)), the diffusion coefficients, D_{ij}, the contravariant base vectors, $\underline{a}^i$, and the moving grid, $(\partial \underline{x} / \partial t)_{\underline{\xi}}$. The time step can be chosen by the user, while the Wiener increment ΔW_j is estimated with a Gaussian random number generator, by putting $\Delta W_j = \sqrt{\Delta t} N_j$, with N_j the realization of a normal random number generator with zero mean and unit variance, e.g., Box-Muller scheme, RIPLEY (1987).

2.3 The Particle Method in Three-Dimensional Free Surface Flows

Many flow models make use of curvilinear boundary-fitted coordinates. Moreover, many nonstationary free surface flow solvers make use of the so-called sigma transformation. The theory developed in section 2.2 will now be applied to a three-dimensional free surface hydrodynamic application which introduces an orthogonal curvilinear grid in the horizontal plane and the sigma-transformation in the vertical. Since the orthogonal curvilinear transformation is only applied in the horizontal plane, it reads:

$$\begin{cases} x_1 = x_1(\xi^1, \xi^2) \\ x_2 = x_2(\xi^1, \xi^2) \end{cases} \tag{2.21}$$

The sigma-transformation is defined as in PHILLIPS (1957):

$$\xi^3 = \sigma = \frac{x_3 - \zeta(x_1, x_2, t)}{H(x_1, x_2, t)} \tag{2.22}$$

with H the water-depth and ζ the water-level elevation above the plane of reference $x_3 = 0$. Now σ-planes may be curved, which implies curved coordinate axes for ξ^1 and ξ^2. More information about the sigma transformation, used in an Eulerian method to simulate a free surface flow, is found in KESTER *et al.* (1989).

Introduce,

$$\begin{aligned} \underline{\alpha}^1 &= \frac{1}{\sqrt{g}} \left(\frac{\partial x_2}{\partial \xi^2}, -\frac{\partial x_1}{\partial \xi^2}, 0 \right)^T \\ \underline{\alpha}^2 &= \frac{1}{\sqrt{g}} \left(-\frac{\partial x_2}{\partial \xi^1}, \frac{\partial x_1}{\partial \xi^1}, 0 \right)^T \end{aligned} \tag{2.23}$$

and let $\sqrt{G_{\xi^i \xi^i}}$ represent the grid cell length along the coordinate line ξ^{3-i} is constant (i=1,2), measured in the Cartesian space, expressed as:

$$\begin{aligned} \sqrt{G_{\xi^1 \xi^1}} &= \sqrt{\left(\frac{\partial x_1}{\partial \xi^1}\right)^2 + \left(\frac{\partial x_2}{\partial \xi^1}\right)^2} \\ \sqrt{G_{\xi^2 \xi^2}} &= \sqrt{\left(\frac{\partial x_1}{\partial \xi^2}\right)^2 + \left(\frac{\partial x_2}{\partial \xi^2}\right)^2} \\ \sqrt{g} &= \sqrt{G_{\xi^1 \xi^1}} \sqrt{G_{\xi^2 \xi^2}} \end{aligned} \tag{2.24}$$

The notation $\sqrt{g}$ may be confusing. It is emphasized that $\sqrt{g}$ represents the two-dimensional analogue of the jacobian, instead of the square root of the acceleration due to gravity. The ξ^1 - and ξ^2 -axes are assumed to be approximately orthogonal, such that:

$$\frac{\partial x_1}{\partial \xi^1}\frac{\partial x_1}{\partial \xi^2} + \frac{\partial x_2}{\partial \xi^1}\frac{\partial x_2}{\partial \xi^2} \approx 0 \tag{2.25}$$

The velocity components, introduced by the hydrodynamic model, are supposed to be transformed to:

$$\begin{aligned} u_{\xi^1} &= \frac{1}{|\underline{\alpha}^1|}\underline{\alpha}^1 \cdot \underline{u} \\ u_{\xi^2} &= \frac{1}{|\underline{\alpha}^2|}\underline{\alpha}^2 \cdot \underline{u} \\ \omega &= u_3 - \frac{1}{\sqrt{g}}(u_{\xi^1}\sqrt{G_{\xi^1\xi^1}}\frac{\partial x_3}{\partial \xi^1} + u_{\xi^2}\sqrt{G_{\xi^2\xi^2}}\frac{\partial x_3}{\partial \xi^2}) - \frac{\partial x_3}{\partial t} \end{aligned} \tag{2.26}$$

Note that the transformed velocity components do not correspond with the contravariant velocity components obtained using tensor analysis, as in (2.8). u_{ξ^1} and u_{ξ^2} remain horizontal velocity components, while ω is the vertical velocity component, relative to a σ-plane. Still, the use of these velocity components will appear to be convenient in the computation of particle displacements in the transformed space.

Since the horizontal mixing processes are not totally understood in shallow water flow problems, three-dimensional hydrodynamic models often assume an isotropic horizontal diffusion. The vertical direction is assumed to be one of the principal directions of the diffusion tensor. Here the diffusion tensor will be written as:

$$D = (D_{ij}) = \begin{pmatrix} D_H(\underline{x},t) & 0 & 0 \\ 0 & D_H(\underline{x},t) & 0 \\ 0 & 0 & D_V(\underline{x},t) \end{pmatrix} \tag{2.27}$$

Application to a more general diffusion tensor is straightforward and will be left out of the discussion.

The procedure sketched in section 2.2, gives rise to the following covariant base vectors:

$$\begin{aligned} \underline{a}_1 &= (\frac{\partial x_1}{\partial \xi^1}, \frac{\partial x_2}{\partial \xi^1}, \frac{\partial x_3}{\partial \xi^1})^T \\ \underline{a}_2 &= (\frac{\partial x_1}{\partial \xi^2}, \frac{\partial x_2}{\partial \xi^2}, \frac{\partial x_3}{\partial \xi^2})^T \\ \underline{a}_3 &= (0\ ,\ 0\ ,\ H(x_1(\underline{\xi}),x_2(\underline{\xi}),t))^T \end{aligned} \tag{2.28}$$

The jacobian of the transformation is expressed as:

$$\sqrt{G} = H\sqrt{g} \tag{2.29}$$

In general, this transformation is nonorthogonal, since $\partial x_3/\partial \xi^i \neq 0$, i=1,2.

$$\begin{aligned} \underline{a}^1 \cdot \underline{a}^2 &= 0 \\ \underline{a}^1 \cdot \underline{a}^3 &= -\frac{1}{HG_{\xi^1\xi^1}} \frac{\partial x_3}{\partial \xi^1} \\ \underline{a}^2 \cdot \underline{a}^3 &= -\frac{1}{HG_{\xi^2\xi^2}} \frac{\partial x_3}{\partial \xi^2} \end{aligned} \tag{2.30}$$

The random walk in the computational domain (i.e., with respect to (ξ^1, ξ^2, σ)) is defined as the simulation of particle trajectories. A path is determined by a one step method given by, i=1,2,3:

$$\begin{cases} \Xi^{i\,(n+1)} = \Xi^{i\,(n)} + (\Delta \Xi^i)^{(n)}_{\text{drift}} + (\Delta \Xi^i)^{(n)}_{\text{random}} \\ \Xi^{i\,(0)} = \Xi^{i\,(0)} \end{cases} \tag{2.31}$$

The start of the sample path is determined by its initial condition corresponding with the initial condition of the advection-diffusion equation. Therefore the initial concentration distribution has to be transformed into an initial condition of the stochastic process (2.3). Details are given in section 3.1.

In this particular case, the dimensionless drift of the particle displacement is given by,

for i=1,2:

$$\begin{aligned} (\Delta \Xi^i)^{(n)}_{\text{drift}} = & \int_{t_n}^{t_{n+1}} \frac{1}{\sqrt{G_{\xi^i\xi^i}}} u_{\xi^i}\, dt \\ & + \left[\frac{1}{G_{\xi^i\xi^i}} \frac{\partial D_H}{\partial \xi^i} + \left(\underline{a}^i \cdot \underline{a}^3\right) \frac{\partial D_H}{\partial \sigma} \right] \Delta t \\ & + \frac{D_H}{\sqrt{G}} \sum_{j=1}^{3} \frac{\partial}{\partial \xi^j} \left[\sqrt{G} \left(\underline{a}^i \cdot \underline{a}^j \right) \right] \Delta t \end{aligned} \tag{2.32a}$$

for i=3:

$$
\begin{aligned}
(\Delta \Xi^3)^{(n)}_{\text{drift}} = & \int_{t_n}^{t_{n+1}} \frac{1}{H}\,\omega\, dt \\
& + \left[\frac{1}{H^2}\frac{\partial D_V}{\partial \sigma} + G_{\xi^1\xi^1}\left(\underline{a}^1\cdot\underline{a}^3\right)\left[\frac{1}{G_{\xi^1\xi^1}}\frac{\partial D_H}{\partial \xi^1} + \left(\underline{a}^1\cdot\underline{a}^3\right)\frac{\partial D_H}{\partial \sigma}\right]\right. \\
& \qquad \left. + G_{\xi^2\xi^2}\left(\underline{a}^2\cdot\underline{a}^3\right)\left[\frac{1}{G_{\xi^2\xi^2}}\frac{\partial D_H}{\partial \xi^2} + \left(\underline{a}^2\cdot\underline{a}^3\right)\frac{\partial D_H}{\partial \sigma}\right]\right]\Delta t \\
& + \frac{D_H}{\sqrt{G}}\sum_{j=1}^{3}\frac{\partial}{\partial \xi^j}\left[\sqrt{G}\left(\underline{a}^3\cdot\underline{a}^j\right)\right]\Delta t
\end{aligned}
\tag{2.32b}
$$

And the dimensionless stochastic displacement becomes,

for i=1,2:

$$
(\Delta \Xi^i)^{(n)}_{\text{random}} = \frac{1}{\sqrt{G_{\xi^i\xi^i}}}\sqrt{2D_H}\,\Delta W_i \tag{2.33a}
$$

for i=3:

$$
(\Delta \Xi^3)^{(n)}_{\text{random}} = \frac{1}{H}\sqrt{2D_V}\,\Delta W_3 + \sum_{i=1}^{2}\left(\underline{a}^i\cdot\underline{a}^3\right)\sqrt{G_{\xi^i\xi^i}}\sqrt{2D_H}\,\Delta W_i \tag{2.33b}
$$

Again the particle suffers a displacement due to the local flow velocity and the space-varying diffusivity. In addition, in the transformed case, nonorthogonality and curvature terms have been introduced to guarantee consistency with the advection-diffusion equation.

Some final remarks:

- The particle displacement in the transformed space is given by

  $\left(\sqrt{G_{\xi^1\xi^1}}\ \Delta \Xi^1, \sqrt{G_{\xi^2\xi^2}}\ \Delta \Xi^2, H\ \Delta \Xi^3\right)^T$.

- The expressions given in (2.32) and (2.33) strongly depend on the assumptions that (i) the transformation is orthogonal in the horizontal plane, i.e., $\left(\underline{a}^1\cdot\underline{a}^2\right) = 0$, and (ii) the diffusion tensor is written as in (2.27), i.e., isotropy in the horizontal plane.

- In stationary flow problems, the moving grid will become fixed in time. It simplifies the expression for the ω - velocity.

- An orthogonal transformation, $\partial x_3 / \partial \xi^i = 0$, i=1,2, simplifies the expressions given in (2.32) considerably. If, in addition, $\left(\partial/\partial \xi^j\right)\left[\sqrt{G}\left(\underline{a}^i\cdot\underline{a}^j\right)\right] = 0\ \ \forall\ i,j$ then the transformed relations become very similar to those expressed in Cartesian

coordinates. This is achieved for grids that are orthogonal, not curved and uniformly stretched.

The numerical aspects of the particle method will be discussed in the next section. The numerical implementation considers:

(i) the representation of the initial condition,
(ii) the deterministic displacement, and
(iii) the stochastic displacement.

3. Numerical Implementation

This section will go into the numerical implementation of the particle method, while using the background flow field, obtained with a hydrodynamic model. The entire process will be illustrated, starting in section 3.1 with the realization of the initial condition and the link between a mass distribution and a concentration distribution. Section 3.2 focuses on the deterministic displacement of particles and finally section 3.3 deals with the stochastic displacement of particles.

3.1 Initial Concentration Distribution

The stochastic process (2.3) is approximated by an ensemble average of sample paths. Each path represents an independent realization of the transport process. The start of a sample path is determined by the initial condition corresponding with the advection-diffusion equation. Therefore the initial concentration distribution has to be transformed to an initial condition of the stochastic process. Discharge problems are easy to handle. Then the starting point of each sample path is located at the discharge point. In general, numerically, the initial concentration distribution will be considered as a sum of delta functions:

$$C_0(\underline{x},t_0) = \sum_{i=1}^{n_c} \overline{C}(\underline{x}_i,t_0)\,\delta(\underline{x} - \underline{x}_i) \tag{3.1}$$

with n_c the number of grid cells, $\overline{C}_i = \overline{C}(\underline{x}_i,t_0)$ the cell averaged concentration value, derived from the initial concentration distribution C_0 and $\underline{x}_i$ the centre of the grid cell. Now the concentration distribution has to be converted into a mass distribution. These two distributions are numerically related by the cell volumes. Therefore the cell volume has to be computed.

Here a grid cell is marked by eight corners (A,B,C,D,E,F,G,H), see figure 3.1, and can be considered as a construction of six pyramids with triangular base (e.g., ABDE, EBDF, EDFH, CBDG, GBDF, GDFH). Since the coordinates of the corners are known, the edges of the pyramids can be determined.

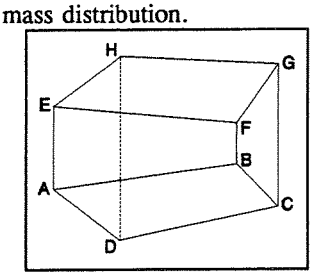

Figure 3.1: Grid cell

For the pyramid ABDE, let:

$$\underline{a}_1 = \vec{AB} \qquad \underline{a}_2 = \vec{AD} \qquad \underline{a}_3 = \vec{AE} \tag{3.2}$$

Define $\varphi : \mathbb{R}^3 \to \mathbb{R}^3$ as:

$$\varphi\underline{x} = (\underline{a}_1\ \underline{a}_2\ \underline{a}_3)\,\underline{x} \tag{3.3}$$

with total derivative

$$D\varphi = (\underline{a}_1 \ \underline{a}_2 \ \underline{a}_3) \qquad (3.4)$$

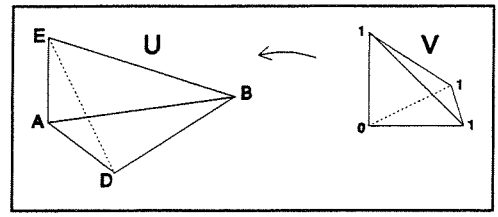

Figure 3.2: The linear mapping of (3.3)

Introduce the open sets U and V (see figure 3.2):

$$\begin{aligned} V &= \{(x_1,x_2,x_3) \in \mathbb{R}^3 \mid 0<x_1<1,\ 0<x_2<1-x_1,\ 0<x_3<1-x_1-x_2\} \\ U &= \varphi(V) \end{aligned} \qquad (3.5)$$

Then, the volume of U is given by:

$$\begin{aligned} \int_U 1\,d\underline{x} &= \int_V |\det(D\varphi)|\ d\underline{x} = \int_0^1 \int_0^{1-x_1} \int_0^{1-x_1-x_2} |\det(D\varphi)|\ d\underline{x} \\ &= \frac{1}{6}\,|\det(D\varphi)| \end{aligned} \qquad (3.6)$$

det(B) denotes the determinant of the matrix B. The volume of a grid cell is approximated with the sum of the volumes of the given six pyramids. If the sides of the grid cell are curved, the outcome of the grid cell volume depends upon the choice of the six pyramids.

Returning to the problem of realizing the initial concentration distribution, particles have to be injected in a grid cell i, $i=1,n_c$, satisfying:

$$\overline{C}_i = (\#\text{ of particles in cell i})*(\text{mass of one single particle}) / (\text{cell volume}) \qquad (3.7)$$

The injection can be performed in various ways. For instance, the particles can be injected at the centre of each grid cell, $\underline{x}_i$, motivated by (3.1), or a uniform injection over each grid cell. The latter approximation corresponds with the approach of deriving a concentration distribution from a mass distribution, by counting the number of particles within a cell. In discharge applications the first approach is the most appropriate. If a continuous initial concentration distribution is given, the second approach is usually applied. Then a finite number of particles are uniformly injected over cell i ($i=1,n_c$) in the transformed space. Unfortunately, in general, a uniform distribution over a grid cell in the transformed space does not imply a uniform distribution over a grid cell in the original space. To inject the particles in the computational domain correctly, each grid cell, as in figure 3.1, is again regarded as the sum of 6 pyramids with triangular base and numerically the initial concentration distribution is considered as the sum of $6n_c$ delta functions. The number of injected particles in each grid cell is again determined by (3.7).

Consider the linear mapping of (3.3) $\varphi : V \to U$. Let $\underline{X}$ have the uniform distribution f:

$$f(\underline{X} = \underline{x}) = \begin{cases} \dfrac{1}{\int_V 1 d\underline{x}} & \underline{x} \in V \\ 0 & \underline{x} \notin V \end{cases} \tag{3.8}$$

It can be proved, by the change-of-variable technique, that the distribution function $\varphi(f(\underline{X} = \underline{x}))$ is also uniform over $\varphi(V) = U$. It is however stated that if grid cells are rectangular the grid cell does not have to be divided into the six pyramids; a uniform injection in the cell is appropriate.

3.2 The Deterministic Displacement

The deterministic displacement of the particle method is defined by equation (2.32) and contains the influence of the local flow velocity, the space-varying diffusivity and curvature (grid stretching). The particle positions do not necessarily coincide with the grid nodes introduced by the grid of the hydrodynamic model. To compute the particle displacements, a continuous velocity field is needed, as well as continuously defined diffusion coefficients.

The contribution of the space-varying diffusivity is easily obtained by finite differencing. For instance, if the diffusivities are known, by the hydrodynamic model, at all centres of the lateral faces of each grid cell, a first order approximation is obtained by taking the diffusivity constant at a lateral face of a grid cell and applying a usual first order finite difference scheme.

As stated, the advection algorithm needs a continuous flow field and various methods can be used. Frequently the 3D flow field is continuously extended by (tri-)linear interpolation, BUNING (1989). Unfortunately, such an interpolation procedure does not guarantee that the continuity equation is satisfied in each point of the continuous space, which implies inconsistency with the physics. Therefore, an extension of the velocity field is proposed, such that the continuity equation is satisfied at each point in the continuous space.

To illustrate the procedure, a normalized two-dimensional grid cell is assumed. Without loss of generality a grid cell is indicated by (0,1)x(0,1), see figure 3.3. The continuous extension of the flow field is now written as, i=1,2:

$$u_i^{ext}(\underline{x},t) = \left(\frac{\partial u_i}{\partial x_i}\right)_{num} x_i + \left(u_i|_{x_i=0}\right)_{num} \quad (3.9)$$

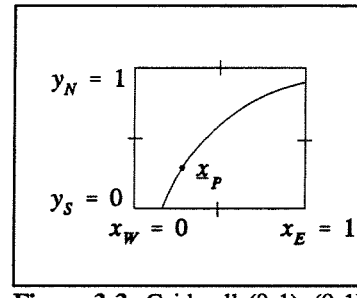

Figure 3.3: Grid cell (0,1)x(0,1)

where $(\partial u_i / \partial x_i)_{num}$ corresponds with the numerical implementation of $\partial u_i / \partial x_i$ as it appears in the continuity equation of the hydrodynamic model. The streamline through $\underline{x} = \underline{x}_p$, can now be obtained exactly within a grid cell, by solving the linear ordinary differential equation analytically, i=1,2:

$$\begin{cases} \dfrac{\partial x_i}{\partial t}(t) = u_i^{ext}(\underline{x},t) \\ x_i(t_0) = (\underline{x}_p)_i \end{cases} \quad (3.10)$$

The divergence of the velocity field equals:

$$\mathbf{div}(\underline{u}^{ext}) = \sum_{i=1}^{2} \frac{\partial u_i^{ext}}{\partial x_i} = \sum_{i=1}^{2} \left(\frac{\partial u_i}{\partial x_i}\right)_{num} = 0 \quad (3.11)$$

A mass conserving hydrodynamic model, which gives the latter equality of (3.11), now implies a mass conserving advection step in the particle model. Furthermore, particles are not able to cross a grid cell boundary where the velocity component normal to this boundary is equal to zero. Another property of the procedure is that the orbit of a particle is not necessarily continuously differentiable with respect to space at grid cell boundaries. The remainder of this section will deal with accuracy and presents some numerical examples. The extension to three dimensions is straightforward.

For convenience, the one-dimensional analogue of (3.10) will be studied. Equation (3.10) observed in one dimension reads, with $t_0 = 0$:

$$\begin{cases} \dfrac{\partial x}{\partial t} = Ax + B \\ x(0) = x_P \end{cases} \quad (3.12)$$

with A and B determined by (3.9). Solving this equation analytically, a distinction between $A = 0$ and $A \neq 0$ has to be made. Here the machine dependent rounding-off error becomes important. Let $u_P = Ax_P + B$. The following table summarizes the possible solutions of (3.12), where x_W and x_E express the left(west)- and right(east)-hand

side of the interval (grid cell), as in figure 3.3 in the two-dimensional case. The three-dimensional case can be treated similarly.

Cases		Time $T_P > 0$ needed to reach cell boundary	position of particle after T_P time
$u_P = 0$		∞	x_P
$A > 0$	$x_P + C > 0$	$\frac{1}{A}\ln\frac{x_E+C}{x_P+C}$	x_E
	$x_P + C < 0$	$\frac{1}{A}\ln\frac{x_W+C}{x_P+C}$	x_W
$A < 0$	$x_W + C > 0$	$\frac{1}{A}\ln\frac{x_W+C}{x_P+C}$	x_W
	$x_E + C < 0$	$\frac{1}{A}\ln\frac{x_E+C}{x_P+C}$	x_E
$A = 0$	$B > 0$	$\frac{x_E-x_P}{B}$	x_E
	$B < 0$	$\frac{x_W-x_P}{B}$	x_W

where $C = B/A$. The logarithms and exponents calculated on a computer are very sensitive for over-flow. Therefore, in computer computations, the different cases have to be treated more carefully. Distinguish the following cases:

1. $|u_P| < \epsilon_1$ instead of $u_P = 0$
2. $|A| < \epsilon_2$ instead of $A = 0$
3. $|B| < \max\{\epsilon_1 , \epsilon_1 - Ax_P\}$ instead of $B = 0$

The solution of (3.12) reads for $A \neq 0$:

$$x(t) = (x_P+C)\exp(At) - C \tag{3.13}$$

and for $A = 0$:

$$x(t) = Bt + x_P \tag{3.14}$$

Note that passing the limit if A tends to zero, the solution of (3.13) converges to that of (3.14). It is concluded that in numerical computations for $0 < |A| \leq \epsilon_2$ and t fixed, the over-all order of accuracy of the solution can not be better than $O(\epsilon_2)$, the machine-dependent rounding-off error.

The coefficients A and B are obtained from a numerical hydrodynamic model and

therefore contain numerical errors. Let A and B represent the analytic values, $\bar{A} = A+\alpha$ and $\bar{B} = B+\beta$ the values produced by the hydrodynamic model. Then $\bar{C} = \bar{B}/\bar{A} = C+\gamma$, $\gamma = O(\alpha,\beta)$, and for fixed t:

$$|x(t) - \bar{x}(t)| = |\gamma - (e^{\alpha t}-1)(x_p+C-\gamma)e^{At}| = O(\alpha,\beta) \tag{3.15}$$

where a bar indicates the numerical method. So, sample paths are realized with an accuracy not better than the accuracy of the computed physical quantities obtained from the hydrodynamic model.

3.3 The Stochastic Displacement

The stochastic contribution of the particle displacement in a free surface flow including the sigma-transformation, is given in (2.33). The diffusion coefficients, showing up in (2.33), are approximated at the particle position with a straightforward (tri-)linear interpolation technique.

It is emphasized that the stochastic particle displacement is determined by the diffusion coefficients D_H and D_V, with D_H the isotropic horizontal diffusivity as expressed in (2.27). If an anisotropic diffusivity is assumed, with principal directions parallel and perpendicular to the main flow direction, the diffusion tensor has to be transformed. Then, in general, the off-diagonal elements of (2.27) become non-zero, which has to be accounted for in the deterministic drift. As a result, the explicit expressions of (2.32) and (2.33) become more complex.

The random Wiener increment can be realized by using a normal random number generator with mean zero and variance Δt, as described in RIPLEY (1987). The computational effort is reduced by approximating $\sqrt{2D_H}\Delta W_i$ with $\sqrt{6D_H\Delta t}R_i$, i=1,2 and a similar expression for i=3, UFFINK (1990). Here R_i represents a uniform random number in (-1,1). The accuracy of the method will hardly be infected by this simplification, since for general nonlinear stochastic differential equations $R(\Delta t) = E([\underline{X}(t+\Delta t) - \bar{\underline{X}}(t+\Delta t)]^2) = O(\Delta t^2)$, RÜMELIN (1982). A bar is written to indicate the numerical method. This convergence (in the mean square limit, see KARLIN and TAYLOR (1975)), can be proved by expanding the sample paths $(\underline{X}(t+\Delta t))$ in a Taylor series, as in RAO *et al.* (1974). Higher order schemes are very hard to get because nonlinear functionals of Gaussian white noise have to be simulated. Higher order schemes (with respect to convergence in distribution), can be obtained by expanding the transition probability density function, as in MILSTEIN (1978) or HAWORTH and POPE (1986). More details about the numerical integration of stochastic differential equations, can be found in GREINER *et al.* (1988) and KLOEDEN (1992).

Since R_i is produced by a computer and therefore defined in a completely deterministic way, it is called a pseudo random number. These pseudo random numbers have to be uniformly distributed, stochastically independent, reproducible, easy to compute and stored with a minimum of memory capacity. Since the results of a random number generator are machine-dependent, a good random number generator does not have

to be good on every computer, e.g., the limited precision of the multiply operation of a 16-bits register computer, differs from the one of a 32-bits register machine.

The mixed congruental generator is given by:

$$r_i = (a r_{i-1} + c) \bmod m \qquad \text{with seed } r_0$$

$$R_i = 2\frac{r_i}{m} - 1 \tag{3.16}$$

Properties of this type of generator together with the stochastic and theoretical tests, have been described in literature, e.g., LEWIS and ORAV (1989) or RUBINSTEIN (1981).

The numerical experiments of section 4 use (appropriate for small computers):

$$\begin{aligned} a &= 5243 \\ c &= 55397 \\ m &= 262139 \end{aligned} \tag{3.17}$$

The computations have been conducted on a workstation HP9000/380 Turbo SRX and a HP9000/720, both equipped with a 32-bits processor. For these computers the cycle-length, the maximum period in (3.16), appeared to be equal to 131069 or 1. Three different cycles can be computed. Starting with the seed 178566 the cycle of length 1 arises. Seed 0 gives rise to a cycle of length 131069, while seed 2 has the same cycle-length (131069) but the produced sequence differs from the sequence computed with seed 0.

LEWIS and ORAV (1989) recommend the following prime-modulus multiplicative generator ($c = 0$, $m = 2^{31}-1$):

$$a = 16807$$

and the five "best" values of a are given by FISHMAN and MOORE (1985):

$$\begin{aligned} a &= 950706376 \\ a &= 742938285 \\ a &= 1226874159 \\ a &= 62089911 \\ a &= 1343714438 \end{aligned}$$

Random walk simulations can be infected by an additional drift, due to the pseudo random number generator. In general, this error can be neglected compared with the time-integration error, the interpolation error, the truncation error and the stochastic error.

4. *Numerical Experiments*

To demonstrate the effectiveness of the particle method, two tests are performed. The first one, described in section 4.1, shows the advection step algorithm of section 3.2 by generating streamlines in the recirculation zone of a channel flow. The second one studies grid-dependency of the particle method applied to a discharge problem in a curvilinear horizontal grid. This example is subjected to section 4.2.

4.1 Streamlines in a Steady Open Channel Flow.

Here a 2DV-application is demonstrated: a stationary channel flow over a threshold. The threshold is positioned in a channel which has a total length of 400m as depicted in figure 4.1. The maximum depth, d, of the channel is 20m and the analytical expression for the threshold reads ($d(x)$ in m):

$$d(x) = \begin{cases} 20 - \dfrac{20}{\pi}\left(1 - \cos\left(\dfrac{\pi(x-15)}{60}\right)\right) & 15\text{m} < x < 135\text{m} \\ 20 & \text{elsewhere} \end{cases} \qquad (4.1)$$

The domain of interest is restricted to the recirculation zone behind the threshold, produced by a hydrodynamic model called TRISULA, TRISULA (1988). The horizontal spatial increment is set to 5m and the vertical water column is divided into 10 layers. The maximum fluctuation in the flow rate is 3.1 10^{-4} m^2/s per unit width (i.e., 0.0024% of initial flow rate). So the flow field is approximately stationary. Figure 4.2 plots the trajectories of two particles, one injected in the recirculation zone, the other released above the top of the threshold. Figure 4.1 shows the computed velocity vectors in the domain of interest. This domain of interest is marked by two vertical lines in the plotted computational domain at the lower part of figure 4.1. The domain $0\text{m} \le x \le 400\text{m}$ is used in the TRISULA program to compute the velocity components, the water-level elevation and the diffusivities with the Prandtl/Schmidt number equal to 1, and a uniform inflow condition with the horizontal velocity component equal to 0.65 m/s.

Figure 4.2 shows that the plotted streamline of the particle in the recirculation zone is indeed closed, which confirms the statements made in section 3.2. The still present fluctuation in the flow rate term does not have any noticeable influence on this result.
A comparison with an analytical solution of the closed orbit is not possible. The particle in the recirculation zone needs 1024s to return to its initial position. The other particle, released above the threshold, left the domain of interest in this time duration. Each second the particle position is plotted. It is very well shown that a particle can not cross a grid cell boundary where the velocity component normal to this boundary is equal to zero, which is valid at closed boundaries, as well as near the centre of a recirculation zone.

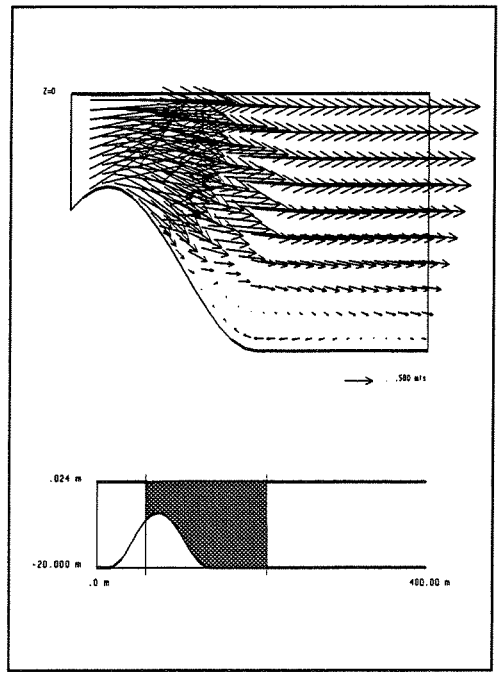

Figure 4.1: Upper part: Velocity field in recirculation zone

Lower part: Computational domain $0\mathbf{m} \leq x \leq 400\mathbf{m}$ and the domain of interest (shaded)

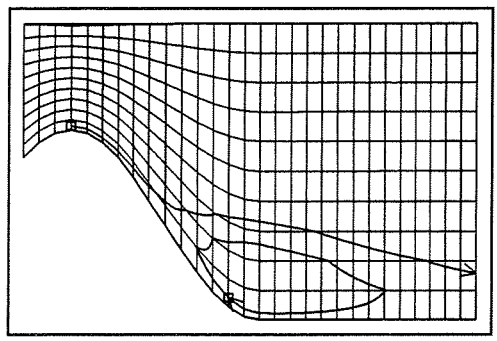

Figure 4.2: Two particle trajectories in a flow over a threshold

4.2 Grid Dependency in the Simulation of a Discharge Problem

Some hydrodynamic models make use of a curvilinear orthogonal transformation. In combination with a finite differencing method, the produced solution is infected with discretization errors. These errors are propagated along the coordinate lines of the introduced grid. Therefore, the produced solution of a hydrodynamic model depends upon

the grid. It should be noted that rectangular grids introduce a similar grid dependency.

This section will study a numerical experiment, which describes the discharge of an initial slug of mass in a 2DH unbounded domain without the presence of a current. If this problem is solved with a finite differencing method which solves the advection-diffusion equation in a curvilinear grid, the polluted region becomes curved and oval shaped, amplified by the steep concentration gradient at initial state. In fact, the solver should produce a circle-shaped polluted region. Therefore, the particle method has been tested to see if the produced solution is also infected by the curved grid. Since the exact solution is known, the particle model will be compared with the analytical solution.

The analytical solution of the (point-) discharge problem, with no mean velocity and constant diffusivity D_H, reads, FISHER *et al.* (1979):

$$C(x_1,x_2,t) = \frac{M/H}{4\pi t D_H} \exp\left(- \frac{(x_1-x_1^c)^2}{4D_H t} - \frac{(x_2-x_2^c)^2}{4D_H t} \right) \tag{4.2}$$

with M the initial mass, H the constant water-depth and (x_1^c, x_2^c) the injection point at $t = 0$. So:

$$C(x_1,x_2,0) = \frac{M}{H} \delta(x_1-x_1^c, x_2-x_2^c) \tag{4.3}$$

$\delta(\underline{x})$ indicates the Dirac-delta function. The particle method can simulate the discharge problem by injecting n_p particles at the exact discharge location (x_1^c, x_2^c). The numerical data read:

H	= 5m,
D_H	= 0.1m^2/s,
n_p	= 400000,
M	= 76kg and
$t = N\Delta t$	= 100s

The numerical grid is constructed such that the coordinate lines along which ξ^1 is constant, coincide with concentric circles (as observed in the Euclidean space). A part of the grid is depicted in figure 4.3. The injection point does not coincide with the origin of the chosen coordinate system. Four tests are conducted:

Test no.	$\sqrt{G_{\xi^1\xi^1}}$ in m	$\sqrt{G_{\xi^2\xi^2}}$ in m	Δt in s
1)	1.0	7.7	1.0
2)	1.0	7.7	0.25
3)	1.96	13.6	4.0
4)	1.96	13.6	1.0

It is noted that $\sqrt{G_{\xi^1\xi^1}}$ is constant throughout the grid, while $\sqrt{G_{\xi^2\xi^2}}$ varies due to curvature. The table contains the averaged grid cell length (and width) of the injected cell. Test 3) and 4) almost double the grid dimensions in comparison with test 1) and 2). It is reminded that the initial number of particles is taken 400000. Increasing the number of particles from 25000 to 100000 resulted in a reduction of the absolute relative error, with respect to test 1), by a factor 2. Therefore the error in the produced solution was still dominated by $O(n_p^{-1/2})$. Taking 400000 particles, the error is mainly due to the time step error.

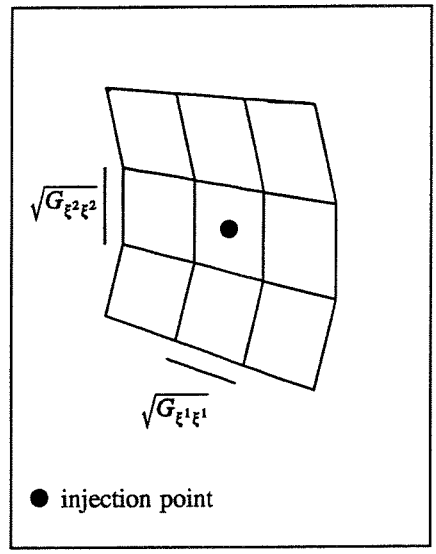

Figure 4.3: Cell dimensions in curved grid

The produced solutions are discussed by observing contour plots and absolute error-measures. The depicted figures (figure 4.4) show two contour lines:

1. The measure of spread of the distribution corresponds with, at $t = N\Delta t$:

$$C = \frac{M/H}{4\pi t D_H} \exp\left(-\frac{1}{2}\right) \tag{4.4}$$

which analytically implies a closed circle as contour line:

$$(x_1 - x_1^c)^2 + (x_2 - x_2^c)^2 = 2D_H t \tag{4.5}$$

2. Grid cells, which contain at least one particle, construct a domain of influence. The boundary of this domain is indicated as a contour line. The corresponding contour value equals half the computed minimum positive cell-averaged concentration value, as observed in the particle method.

The numeric error, at $t = N\Delta t$, is written as:

$$\epsilon_i(\overline{C}) = |C_i - \overline{C_i}| \tag{4.6}$$

C_i denotes the concentration value generated by the particle method. $\overline{C_i}$ equals the mean concentration of cell i, obtained by numerical integration of expression (4.2). Results of test 1) are illustrated in figure 4.4. The error measure has been summarized in the following table. The contour plots of test 2), 3) and 4) are omitted.

Test no.	$\overline{C}(x_1^c, x_2^c, N\Delta t)$	$\sum_{i=1}^{nc} \lvert C_i - \overline{C}_i \rvert$
1)	0.538	0.452
2)	0.541	1.2124
3)	0.421	0.075
4)	0.436	0.088

Analytically: $\overline{C}(x_1^c, x_2^c, N\Delta t)$ = 0.537 (fine grid, test 1) and 2))
$\overline{C}(x_1^c, x_2^c, N\Delta t)$ = 0.428 (course grid, test 3) and 4))

Now define the factor α, acting as a Courant number, as:

$$\sqrt{6\,\Delta t D_H} = \alpha \min_{i \in \{1,..,nc\}} \left(\sqrt{G_{\xi^1\xi^1}}_i, \sqrt{G_{\xi^2\xi^2}}_i \right) \tag{4.7}$$

Test 1) and 3) are executed with Δt such that $\alpha = 0.78$. It will be shown that for a fixed curvilinear grid, the optimal accuracy can be obtained if Δt is chosen such that $\alpha \approx 1$. Observing the error measure of the particle method, time step reduction does not benefit the final result. It is already noted that the error is not dominated by the (finite) initial number of particles. So, an increase of n_p for test 2) or 4) will not improve the result. Here the error is due to the horizontal curvature terms. In the particle model these terms are ignored, since $(\underline{a}^1 \cdot \underline{a}^2) = 0$ is assumed. Decreasing Δt (still requiring $\alpha \leq 1$) will not add more information about the curvature since the defined grid remains unchanged. Only the computation time will increase proportionally. Locally, the curved coordinate lines are approximated with straight lines parallel to the covariant base vectors (the grid cell edges). A particle travels Δt time in a direction which is a linear combination of these two base vectors. The base vectors are taken locally constant and will only be adapted when a particle crosses a grid cell boundary. Therefore, a particle

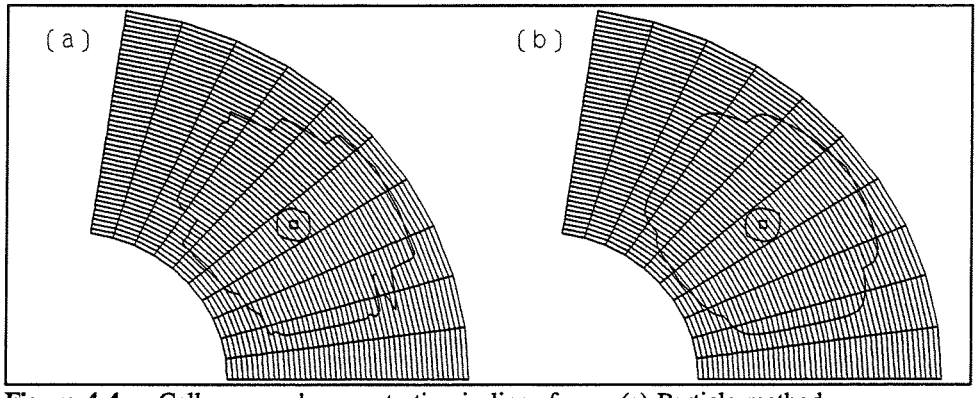

Figure 4.4: Cell averaged concentration isolines for (a) Particle method
(b) Analytical computations

that moves within a grid cell, is not aware of the curvature of the grid, although its position is directly related to the grid. Neglect of curvature during the travelling time Δt, will introduce an error. Whenever a particle crosses a grid cell boundary, the particle continues its walk with respect to the base vectors determined at the intermediate station. For reasons of resolution, α is also restricted: $\alpha < 1$, i.e., a particle crosses at the most one grid cell boundary per time step. Therefore, optimal results will be obtained for $\alpha \approx 1$. It is concluded that grid dependency can not be avoided, while using approximate orthogonal curvilinear grids. Note that in a rectangular equidistant grid (in the absence of curvature terms), grid dependency is determined by equation (4.7).

Grid Dependency of the Plotting Routine

Plots are frequently used to support the interpretation of the computational results. If a contour plot of constant concentration values shows a grid dependency, it is sometimes not immediately clear that this is due to the plotting routine or due to the computational method that solved the concentration field. The previous paragraph explains that grid dependency is present in the particle method. The plotting routine however amplifies the grid dependency in the depicted figures (figure 4.4). In general, numerical methods produce a discrete concentration field specified at the grid nodes. The plotting routine uses this information and applies a linear interpolation technique within, for instance, a quadrangle. In a coarse grid, such as the one described in test 1), the contour line results in a slightly misleading plot. In figure 4.4(b) the analytical information restricted to the grid nodes has been used. Therefore the expected closed concentric circles can not be recognized. This deficiency can be overcome if the discrete concentration field can be continuously extended. Then the plotting routine can be applied at a much finer grid, without repeating the numerical computations that solves the concentration field. In the analytical case, the concentration field is known at every point in space, given by equation (4.2), and a grid refinement in the plotting routine results in figure 4.5(b). It is noted that the contours of the constant concentration values are plotted, while in figure 4.4 the contour of constant cell-averaged concentrations are depicted.

A continuous concentration can also be obtained while using a particle method. Cell-averaged concentration values can simply be obtained by counting the number of particles within a fixed grid, as noted in section 3.1. It is also possible to apply other methods to convert the mass density of the discrete particles into concentrations. The one described here sums the significant particle influences in the vicinity of the calculation point $\underline{x}$ with a particular mass distribution φ centred on the particle locations $\underline{X}^p$, i.e.,

$$C(\underline{x},t) = \sum_{p=1}^{n_p} \varphi(\underline{x}-\underline{X}^p(t),t) \tag{4.8}$$

In the 2DH discharge application, the following extended continuous concentration field has been applied:

$$C(x_1,x_2t) = \frac{1}{H}\sum_{p=1}^{n_p} \mu_p \; \varphi(x_1 - X_1^p(t),t;\sigma_{x_1}) \; \varphi(x_2 - X_2^p(t),t;\sigma_{x_2}) \tag{4.9}$$

with μ_p the mass of one single particle and

$$\varphi(\eta,t;\sigma) = \frac{1}{\sqrt{2\pi}\sigma}\exp\left(-\frac{1}{2}\left(\frac{\eta}{\sigma}\right)^2\right) \tag{4.10}$$

This, so-called point-spread function φ contains one degree of freedom given by σ. The variance, σ^2, still has to be specified. BOOGAARD (1992) states that in one-dimensional applications, σ is proportional to $n_p^{-1/5}$ (as $n_p \to \infty$) and moreover σ is proportional to $\sqrt{t}$. Writing

$$\sigma = \beta \; n_p^{-1/5} \sqrt{t} \tag{4.11}$$

β can be approximated by minimizing:

$$E\left[\int_{-\infty}^{\infty}\left[C(\eta,t) - \sum_{p=1}^{n_p}\varphi(\eta - X^p(t),t;\sigma)\right]^2 d\eta\right] \tag{4.12}$$

with respect to σ. The expectation E represents an ensemble average of I samples of X^p. C in (4.12) is gaussian distributed with mean zero and variance $2D_H t$. A computer simulation yields, with I = 15, $\beta^{opt} = 1.09308$, such that

$$\sigma_{x_1} = \sigma_{x_2} = \beta^{opt}\frac{\sqrt{2D_H t}}{(n_p)^{1/5}} \tag{4.13}$$

It is noted that the choice of β influences the smoothed mass distribution. As illustrated by MONTMINY *et al.* (1992) a small value of β, $\beta < \beta^{opt}$, does not yield a smooth concentration distribution, while a large β, $\beta > \beta^{opt}$, exaggerates the width of the global distribution. Applying (4.13) gives reasonable and adequate results.

Finally the plotting routine can be applied on a much finer grid than the one used in figure 4.4, since (4.9) and (4.13) approximates the concentration field at every point in space. This procedure results in figure 4.5 where the contour values are given by

$C_1 = 0.3669227$ kg/m^3, and
$C_2 = 0.0000307$ kg/m^3

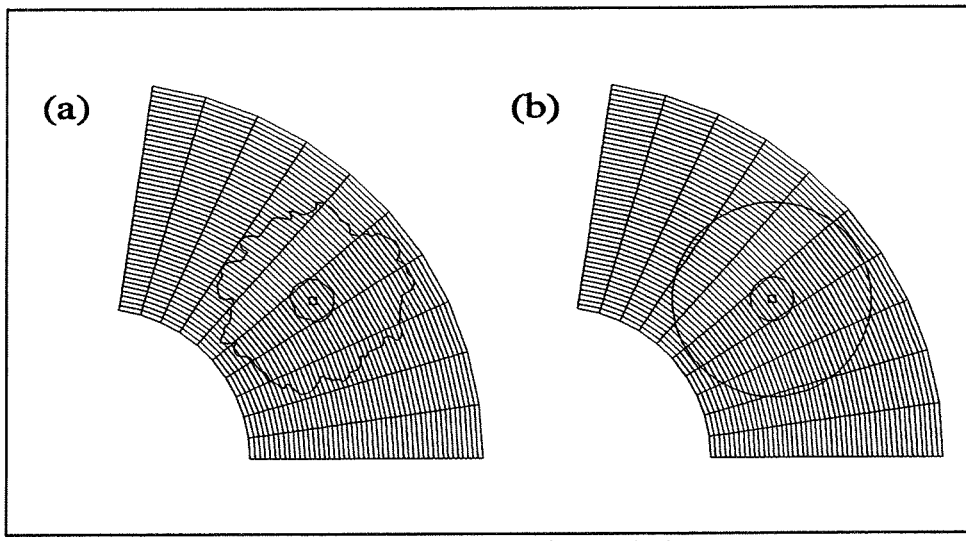

Figure 4.5: Concentration isolines for (a) Particle method
(b) Analytical computations

5 Conclusions

This paper provides a numerical description for solving the advection-diffusion equation, by using particle tracking, while taking into account the available discrete flow information. Formulas for the drift and random particle displacements, computed in a curved nonorthogonal grid are given. The discrete flow field has been continuously extended such that the streamlines are solved analytically with respect to the extended flow field. It has been observed that grid dependency is noticeable in assumed orthogonal curvilinear applications. Since visualization techniques are also grid dependent, plots can be slightly misleading in concluding grid-dependency. Using curvilinear grids, the optimal time step is determined by equation (4.7) with $\alpha \approx 1$, with respect to accuracy, resolution and computation time.

Appendix A: Transformation Relations

Curvilinear boundary fitted coordinates are frequently used to solve fluid flow problems. This transformation approach is introduced from a numerical point of view. Although the transformation from a Cartesian coordinate system to such a curvilinear coordinate system results in more complex differential equations, it is possible to derive convenient and accurate discretization methods in the transformed space. If a particle method is used in combination with a fluid flow solver, dealing with curvilinear coordinates, the trajectory can be computed in the transformed space, as explained in section 2. The derivation will be summarized in this appendix by listing the necessary transformation relations. These relations correspond with those listed in section 2.2.1. General comments about and derivation of the transformation relations can be found in THOMPSON *et al.* (1985) or CUVELIER (1987).

For a scalar function C, such as concentration, partial derivatives with respect to both coordinate systems, (x_1,x_2,x_3) and (ξ^1,ξ^2,ξ^3), are related by:

$$\frac{\partial C}{\partial x_j} = \sum_{i=1}^{3} \frac{\partial C}{\partial \xi^i}\frac{\partial \xi^i}{\partial x_j} = \sum_{i=1}^{3} (\underline{a}^i)_j \frac{\partial C}{\partial \xi^i} = \frac{1}{\sqrt{G}} \sum_{i=1}^{3} \frac{\partial}{\partial \xi^i}\left[\sqrt{G}(\underline{a}^i)_j C\right] \tag{A1}$$

The first equality of (A1) is explained by the chain rule. The second equality uses the definition of the contravariant base vectors (2.7) and the third equality expresses the conservative form of the derivative of a scalar quantity with $\sqrt{G}$ the jacobian of the transformation (2.7). Note that the overall conservation of a transported quantity is guaranteed when the numerical method deals with a conservative description of the equations. The following identity has been used to obtain conservative expressions:

$$\sum_{i=1}^{3} \frac{\partial}{\partial \xi^i}\left[\sqrt{G}\underline{a}^i\right] = \underline{0} \tag{A2}$$

This identity can be proved with the divergence theorem applied to an infinitesimal element and reminding that the vector normal to the faces of this infinitesimal element is given by the contravariant base vector.

If a moving grid is applied, the time derivatives also have to be transformed. The expression for the time derivative becomes:

$$\left(\frac{\partial C}{\partial t}\right)_{\underline{\xi}} = \left(\frac{\partial C}{\partial t}\right)_{\underline{x}} + \nabla C \cdot \left(\frac{\partial \underline{x}}{\partial t}\right)_{\underline{\xi}} \tag{A3}$$

where the subscripts indicate the variable which is held constant. In particular

$$\left(\frac{\partial \xi^i}{\partial t}\right)_{\underline{x}} = -\sum_{j=1}^{3} (\underline{a}^i)_j \left(\frac{\partial x_j}{\partial t}\right)_{\underline{\xi}} \tag{A4}$$

Finally (A1) gives rise to the following relations:

$$\nabla C = \frac{1}{\sqrt{G}} \sum_{i=1}^{3} \frac{\partial}{\partial \xi^i} \left[\sqrt{G}\, \underline{a}^i C\right] \tag{A5}$$

And

$$\nabla \cdot \underline{u} = \frac{1}{\sqrt{G}} \sum_{i=1}^{3} \frac{\partial}{\partial \xi^i} \left[\sqrt{G}\, \underline{a}^i \cdot \underline{u}\right] \tag{A6}$$

Substitution of these expressions in the advection-diffusion equation (2.1) is straightforward and it results immediately in the transformed advection-diffusion equation as expressed in (2.14). The transformed Fokker-Planck equation, given by (2.15), is obtained similarly.

Appendix B: References

ARNOLD L. (1974)
Stochastic differential equations: theory and applications.
John Wiley and Sons.

BOOGAARD H.F.P. van den, M.J.J. HOOGKAMER and A.W. HEEMINK (1992)
Parameter identification in particle models.
submitted to *Stochastic Hydrology and Hydraulics.*

BUNING P.G. (1989)
Numerical algorithms in CFD post-processing.
Von Karman Institute for Fluid Dynamics, Lecture series 1989-07.

CORRSIN S. (1974)
Limitations of gradient transport models in random walks and in turbulence.
Advances in Geophysics, Vol.18A, pp25-60.

CUVELIER C. (1987)
Differential equations of viscous fluid flow in general coordinates.
Delft University of Technology, department of mathematics, lecture notes.

DRONKERS J., A.G. VAN OS and J.J. LEENDERTSE (1981)
Predictive salinity modeling of the Oosterschelde with hydraulic and mathematical models.
In: *Transport models for inland and coastal waters*, H.B. FISCHER, editor, Academic Press, New York, pp. 451-482.

DURBIN P.A. (1983)
Stochastic differential equations and turbulent dispersion.
NASA Reference Publication 1103.

FELLER W. (1971)
An introduction to probability theory and its applications.
Volume II, second edition. John Wiley, New York.

FISCHER H.B., E.J. LIST, R.C.Y. KOH, J. IMBERGER and N.H. BROOKS (1979)
Mixing in inland and coastal waters.
Academic press, New York.

FISHMAN G. and L. MOORE (1985)
An exhaustive analysis of multiplicative congruential random number generators with modulus 2^{31}-1.
SIAM Journal of Scientific and Statistical Computing, Vol.7, No.1, pp24-25.

FORESTER C.K. (1977)
Higher order monotonic convective difference schemes.
Journal of Computational Physics, Vol.23, pp1-22.

GREINER A., W. STRITTMATTER and J. HONERKAMP (1988)
Numerical integration of stochastic differential equations.
Journal of Stochastic Physics, Vol.1, No.1/2, pp95-108.

HAWORTH D.C. and S.B. POPE (1986)
A second-order Monte Carlo method for the solution of the Itô stochastic differential equation.
Stochastic Analysis and Applications, Vol.1, No.2, pp151-186.

HEEMINK A.W. (1990)
Stochastic modelling of dispersion in shallow water.
Stochastic Hydrology and Hydraulics, Vol.4, pp161-174.

JAZWINSKI A.H. (1970)
Stochastic processes and filtering theory.
Academic press, Inc., New York.

KAMPEN N.G.van (1981a)
Stochastic processes in physics and chemistry.
North-Holland Publishing Company.

KAMPEN N.G.van (1981b)
Itô versus Stratonovich.
Journal of Statistical Physics, Vol.24, No.1, pp175-187.

KARLIN S. and H.M. TAYLOR (1975)
A first course in stochastic processes.
Second edition, Academic Press, Inc., New York.

KESTER J.van, G.S. STELLING and R.E. UITTENBOGAARD (1989)
The σ-coordinate transformation and the basic equations of TRISULA.
Estuaries and seas division, Delft Hydraulics.

KLOEDEN P.E. and E. PLATEN (1989)
A survey of numerical methods for stochastic differential equations.
Stochastic Hydrology and Hydraulics, Vol.3, pp179-190.

KLOEDEN P.E. and E. PLATEN (1992)
Numerical solution of stochastic differential equations.
Springer-Verlag, Berlin, Heidelberg.

LEWIS P.A.W. and E.J.ORAV (1989)
Simulation methodology for statisticians, operations analysts and engineers.
Vol. 1, Wadworth and Brooks/Cole, Pacific Grove.

MILSHTEIN G.N. (1978)
A method of second-order accuracy integration of stochastic differential equations.
Theory of Probability and its Applications, Vol.23, pp396-401.

MONTMINY M., M. LECLERC, G. MARTIN and P. BOUDREAULT (1992)
PANACHE: An interactive software to simulate steady-state two-dimensional transport-diffusion of pollutants in rivers using a particle tracking method.
Computer Techniques and Applications, Fourth international conference on hydraulic engineering software hydrosoft/92, pp27-38.

PHILLIPS N.A. (1957)
A coordinate system having some special advantages for numerical forecasting.
Journal of Meteorology, Vol.14, pp184-185.

RAO N.J., J.D. BORWANKARAN and D. RAMKRISHNA (1974)
Numerical solution of Itô integral equations.
SIAM Journal on Control, Vol.12, No.1, pp124-139.

RIPLEY B.D. (1987)
Stochastic simulation.
John Wiley & Sons, New York.

RISKEN H. (1984)
The Fokker-Planck equation.
Springer Verlag, Berlin.

RUBINSTEIN R.Y. (1981)
Simulation and the Monte Carlo method.
Wiley, New York.

RÜMELIN W. (1982)
Numerical treatment of stochastic differential equations.
SIAM Journal on Numerical Analysis, Vol.19, No.3, pp604-613.

THOMPSON J.F., Z.U.A. WARSI and C.W. MASTIN (1985)
Numerical grid generation: foundations and applications.
North-Holland, Amsterdam.

TRISULA (1988)
Trisula documentation guide.
Version 0, Delft Hydraulics, Delft.

UFFINK G.J.M (1990)
Analysis of dispersion by the random walk method.
Dissertation of Doctor's thesis, Delft.